In-situ estimation of acoustic impedance on the surfaces of a room for inverse sound rendering

Gabriel Pablo Nava, Yosuke Yasuda, Yiochi Sato, Shinichi Sakamoto
Institute of Industrial Science, The University of Tokyo.
4-6-1 Komaba, Meguro-ku, Tokyo, 153-8505, Japan.
e-mail: {**pablo, yyasuda, ysato, sakamo**}**@iis.u-tokyo.ac.jp**

Abstract

We present a method based on the inverse boundary element method (IBEM) for the in-situ estimation of normal acoustic impedances of the surfaces in a room. As input to the inverse process, this technique uses the geometry of the interior space, the position and strength of the sound source, and a set of sound pressures measured at random positions in the acoustic field. Previous work in inverse radiation problems has employed computational expensive techniques such as singular value decomposition (SVD) in order to obtained satisfactory results. In contrast, the numerical simulations of the present work show that the least-squares approach can give satisfactory solutions when the linear system of the formulation derived here is sufficiently overdetermined with sound samples taken at random locations in the interior. The use of 3D stereo vision tracking is suggested to enable the practical measurement of large sets of field pressures. Currently, *inverse sound rendering* for virtual reality (VR) is a targeted application of our method.

1 Introduction

Prediction of sound fields with numerical methods has been widely used for noise control, acoustic building design and recently for sound rendering of virtual reality environments. These methods often require the specification of boundary conditions that characterize the acoustic properties of the materials. For example, once the acoustic impedances of the materials are known, numerical analysis such as boundary or finite element methods can be applied to predict and control the sound field by manipulation of the analyzed materials. However, there are situations in which it is not always possible or desirable to take samples of the materials to the laboratory for proper measurements, and instead their acoustic characteristics have to be estimated in their original location.

A number of in-situ measurement methods have been proposed since around seven decades ago. A well documented survey on in-situ measurements of acoustic absorption and impedance was done by Noke and Mellert, [1]. But it was not until recent years that in-situ measurement techniques based on inverse acoustic numerical methods attracted the interest of researchers due to their applicability to arbitrary geometries. In such methods the underlying idea is that it is possible to reconstruct the boundary parameters of the vibro-acoustic system if there is a transfer function or a propagation model that relates the sound field with the boundaries. The reconstruction is then achieved by solving the inverse problem in the least-squares sense using samples of sound taken at reference points in the field. In the present work the inverse boundary element method (IBEM) is used as backpropagation model for the estimation of acoustic impedance of the boundaries, which is achieved by a simultaneous calculation of the sound pressure and the particle velocity of the steady-sate vibrating surfaces of a closed geometry.

The idea of inverse reconstruction of surface parameters in acoustic radiation problems was widely spread perhaps with the appearance of the near-field acoustic holography (NAH) technique, introduced by Maynard *et. al.*, [2],[3], and subsequently followed by other research on that subject, e.g. [5][6][7]. In NAH, estimation of the sound source strength is performed by placing a plane array of sensors (hologram) in the near-field

of the vibrating source and using the sampled data to solve the discretized Kirchoff-Helmholtz equation.

Extensive work and improvements have been done in that area, but in contrast a few researhers have recently started to tackle the inverse acoustic interior problem in which the boundary values of an enclosed space are sought given the geometry and a set of field pressure samples. For example Kim and Ih, [10], presented a method based on the boundary element method (BEM) for the reconstruction of the vibro-acoustic parameters in the interior of car panels.

As previous research has reported, the solution to this kind of acoustic inverse problems is typically ill-conditioned, and in most cases the use of singular value decomposition (SVD) together with a regularization step and optimal placement of the sensors is required in order to ensure an acceptable accuracy of the reconstructed boundary parameters. The use of SVD has been made by early investigations on NAH, [4], and later by a number of researchers, e.g. [5], [13], [14]. Tikhonov regularization, [15], has also been used by other approaches to the inverse reconstruction problem, [8], [9], [11]. In those studies, the noise in the measurements affecting the ill-conditioning of the problem, has been taken as the main source of error. In this work, we will consider other sources of error such as the vibration modes and the mesh quality which were found to affect the accuracy even in the absence of noise. Moreover, since the analysis based on SVD is computationally expensive, we have tested the application of other linear solvers such as Gaussian elimination and least-squares to solve the inverse estimation problem using the method derived here.

Another aspect of concern is the placement of the measurement points. Nelson and Yoon, [8],[9], have suggested that the best reconstruction of source strength in radiation problems is achieved when the samples of field sound are taken close to the surfaces, following the shape of the geometry and with a separation equal to that of the discretized sound sources. In a further work Kim and Ih, [11], suggested the use of the effective independence method (Efi) for the optimal selection of the sound field sensor whose positions minimize the norm error in the back reconstruction, and showed an application example of a half-scaled car cabinet. In general, these approaches have shown satisfactory results when the measurement points have been carefully placed. But in the practical point of view, it is difficult to achieve such a strict optimal placement of microphones in the acoustic field when we deal with large and complex geometries, for example real room. Therefore in the present work, simulations of the inverse estimation of acoustic impedances from field pressures at random locations will be considered.

We emphasize the application of IBEM to the in-situ estimation of surface impedances by exploiting *a priori* knowledge of the surface segmentation to provide the system with more information about the desired solution. At the end of the present work, the derivation of a weighted least-squares with an extra constraint imposed by the surface segmentation will be presented. Finally, while previous work, [11], have concentrated on the reconstruction of vibro-acoustic parameters in interiors for the detection of noise sources, the targeted application of our method is *inverse sound rendering* for virtual reality, in which engineers wish to acquire the acoustic properties of the real world objects so they are able to reproduce realistic and novel sound fields under new geometric configurations in the virtualized models. An introduction to this concept in the computer graphics area can be found in [18].

2 In-situ estimation of acoustic impedance with IBEM

Similarly to the inverse radiation problems, the estimation of the acoustic impedance of the interior surfaces $S_1, S_2, ..., S_n$ of an enclosed space (e.g. a room) involves the solution of an inverse model and a set of sound samples measured in the interior field. In other words, given the geometry of the space, the strength and position of a time-harmonic sound source (e.g. a speaker with a sinusoidal tone) placed somewhere in the enclosing shape, and a set of sound pressures taken at known locations in the acoustic field, the problem is to find the acoustic impedance values at the boundaries (i.e. the surfaces). Figure 1 summarizes this inverse estimation problem.

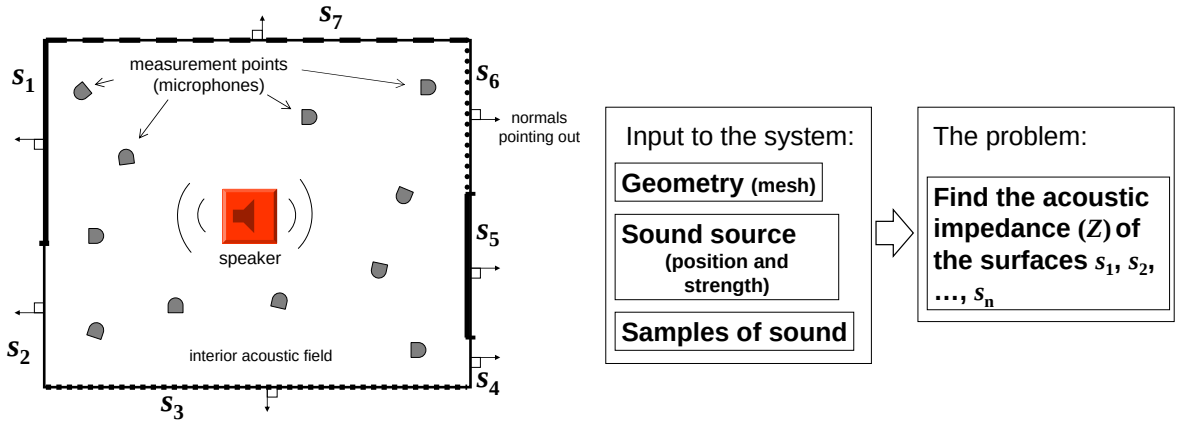

Figure 1: The problem of inverse estimation of the acoustic impedances.

At the boundaries of the surfaces $S_1, S_2, ...S_n$, the acoustic impedance can be expressed by the relation

$$Z_{s_l}(\vec{r},\omega) = \frac{p_{s_l}(\vec{r},\omega)}{v_{s_l}(\vec{r},\omega)} \tag{1}$$

where $p_{s_l}(\vec{r},\omega)$ and $v_{s_l}(\vec{r},\omega)$ denote respectively the sound pressure and particle velocity at the position $\vec{r}$ for the frequency ω. In the subsequent analysis the frequency and the position factors will be omitted for simplicity and because we will be dealing with steady-state analysis. Hence, estimation of the impedance at the boundaries is equivalent to finding the sound pressure p_S and particle velocity v_S of the interior surfaces. Kim and Ih, [11], have already shown that employing the IBEM, it is possible to approach this problem.

In the formulation of the acoustic BEM for an interior analysis [16], discretization of a closed surface into N elements yields to the discrete form of the Kirchhoff-Helmholtz equation which relates p_S and v_S with the sound pressure in the field p_f, as expressed by

$$c_f p_f + \sum_{i=1}^{N} p_{S,i} a_i - \sum_{i=1}^{N} v_{S,i} b_i = 0 \tag{2}$$

where c_f is a constant equal to $1/(4\pi)$ times the solid angle through which the evaluation points sees the surface, [16]. The influence coefficients a_i and b_i are given by

$$a_i = \sum_{l=1}^{N} \int_{S_l} \mathrm{R}_{il} \partial_n \mathrm{G}(\vec{r}) dS$$

$$b_i = -j\omega\rho \sum_{l=1}^{N} \int_{S_l} \mathrm{R}_{il} \mathrm{G}(\vec{r}) dS$$

$$\mathrm{G}(\vec{r}) = \frac{e^{-jkr}}{4\pi r}$$

Here, j is the imaginary number operator, ρ the density of the acoustic media ($\simeq 1.21 kg/m^3$ for air), k the wave number, $\mathrm{G}(\vec{r})$ is the Green's function in free space with $r = \|\vec{r}\|$, ∂_n denotes partial differentiation with respect to the normal vector of the surface, and R_{il} is an interpolation function. In the present work, triangular elements with constant interpolation are considered, and the surface integrals are approximated with Gaussian quadrature integration. By using a collocation technique and a set of sound pressures at M field points, it can be shown, [16], that two basic BEM equations can be written in a matrix form as follows:

$$\mathbf{A}_S \mathbf{p}_S = -j\omega\rho \mathbf{B}_S \mathbf{v}_S \tag{3}$$

$$\mathbf{C}\mathbf{p}_f + \mathbf{A}_f \mathbf{p}_S = -j\omega\rho \mathbf{B}_f \mathbf{v}_S \tag{4}$$

$\mathbf{A}_S$ and $\mathbf{B}_S$ are $N \times N$ surface-surface influence matrices, and similarly $\mathbf{A}_f$ and $\mathbf{B}_f$ denote $M \times N$ surface-field influence matrices. $\mathbf{p}_S$ and $\mathbf{v}_S$ are vectors of the surface pressures and velocities respectively, and $\mathbf{C}$ is an $M \times M$ identity matrix since the pressures $\mathbf{p}_f$ are measured inside the acoustic field.

As discussed above, the geometry and the location of the field points $\mathbf{p}_f$ are known, therefore the influence matrices $\mathbf{A}$'s and $\mathbf{B}$'s can be computed in advance. Also information of the sound source strength (vibration amplitude of the speaker) is known, thus equations (3) and (4) can be rewritten giving:

$$\mathbf{A}_S\mathbf{p}_S + j\omega\rho\tilde{\mathbf{B}}_S\tilde{\mathbf{v}}_S = -j\omega\rho\hat{\mathbf{B}}_S\hat{\mathbf{v}}_S \tag{5}$$

$$\mathbf{A}_f\mathbf{p}_S + j\omega\rho\tilde{\mathbf{B}}_f\tilde{\mathbf{v}}_S = -j\omega\rho\hat{\mathbf{B}}_f\hat{\mathbf{v}}_S - \mathbf{C}\mathbf{p}_f \tag{6}$$

In equations (5) and (6) the unknown and known parameters have been separated, where $\mathbf{p}_S$ and $\tilde{\mathbf{v}}_S$ are the unknown pressures and velocities of the surfaces and their corresponding influence coefficients $\mathbf{A}$'s and $\tilde{\mathbf{B}}$'s. $\hat{\mathbf{v}}_S$ are the known velocities of the vibrating surface of the sound source with their influence coefficients $\hat{\mathbf{B}}$. It is readily noted that equations (5) and (6) form a linear system with two unknowns that can be solved by combining both equations and then using SVD-based analysis yields to one of the least-square solutions, [8],[11]. Recalling that the parameter that we wish to estimate is the acoustic impedance given by (2), we attempt to find a solution for both $\mathbf{p}_S$ and $\mathbf{v}_S$ simultaneously by rewriting the linear system of equations (5) and (6) in the form

$$\begin{pmatrix} \mathbf{A}_S & j\omega\rho\tilde{\mathbf{B}}_S \\ \mathbf{A}_f & j\omega\rho\tilde{\mathbf{B}}_f \end{pmatrix} \begin{pmatrix} \mathbf{p}_S \\ \mathbf{v}_S \end{pmatrix} = -j\omega\rho \begin{pmatrix} \hat{\mathbf{B}}_S\hat{\mathbf{v}}_S \\ \hat{\mathbf{B}}_f\hat{\mathbf{v}}_S - \frac{j}{\omega\rho}\mathbf{C}\mathbf{p}_f \end{pmatrix} \tag{7}$$

which we compactly express as

$$\mathbf{D}\mathbf{x}_S = \mathbf{d} \tag{8}$$

Now the inverse estimation process can be done by taking $M \geq N$ measurements of field pressures $\mathbf{p}_f$ and obtaining the least-squares solution of equation (8). In the following section we will present a numerical simulation comparing results obtained with Gaussian elimination and least-squares with those obtained by including Tikhonov regularization to the least-square solution suggested in previous work, [8] , [16].

One can argue that the solution of the augmented system of equation (8) involves unnecessary computational effort, however as it will be discussed in the future work section, this formulation of the inverse problem allows us to impose an extra constraint to the least-squares solution.

3 Numerical simulations

3.1 Realistic geometry: scaled office room

The first 3D model used for the application of the inverse estimation of acoustic impedances consists of a realistic geometry taken from an empty office room. The model is scaled 1:4 and its mesh is built using triangular elements. Figure 2 shows the scaled model of the office. The resulting mesh is composed of 414 elements ($N = 414$) with a maximum edge size of 0.168 m. Following the criterion of $1/6$ of a wavelength the mesh can be used in simulations for frequencies up to 340 Hz. However we limit the analysis to the range of 10–250 Hz. In the first stage of all the simulations a number of field pressures is artificially generated at M points randomly distributed in the room, as illustrated in the example of Figure 3. The field pressures are calculated by a BEM process in which acoustic impedances have been assigned manually to the boundaries. For simplicity and appreciation of the accuracy in the back reconstruction, real valued impedances have been applied to all the surfaces. Table 1 shows the type of materials applied to the surfaces and their impedance values which were taken from a database [17]. Note therefore, that they are not the original values of the real office but they are useful for our test purposes. A sound source was simulated by placing the model of a boxed speaker in one corner of the room. The vibrating surface of the speaker displaces with an amplitude of particle velocity of 1 m^3/s. It is clear that vibration modes appear within the range of analysis frequencies, however the effects of the vibration modes will be discussed and illustrated in a further example.

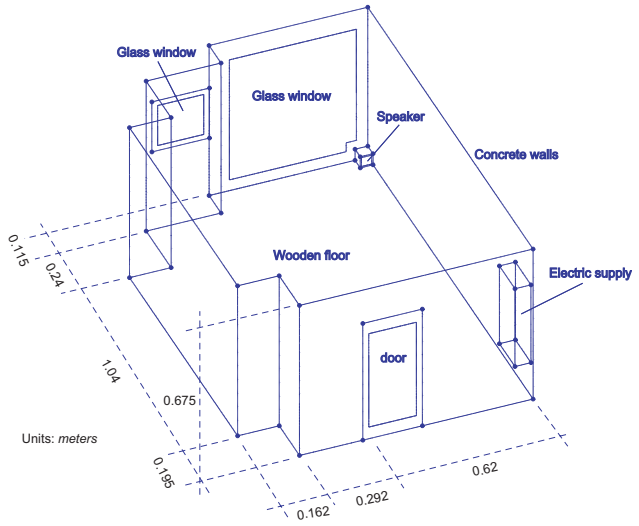

Figure 2: Scaled model of the office room.

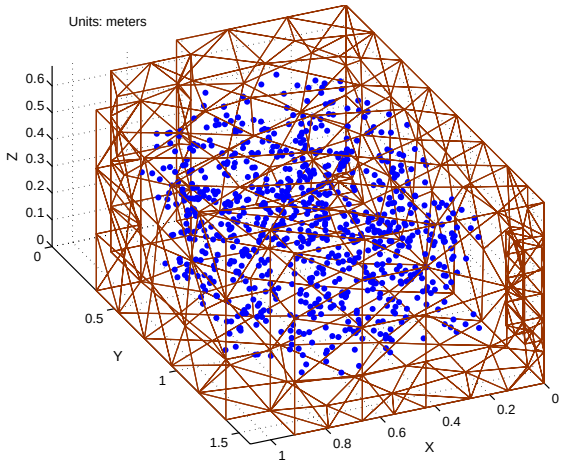

Figure 3: Mesh and randomly distributed field points.

The generated set of field pressures is used in the inverse process defined in equation (8) to recover the designated impedances . Although previous work, [8], [11], has included levels of simulated noise, in the present study noise has been omitted in the field pressures since we are investigating at this stage the degree of error introduced by the proposed formulation of the problem in its elemental form.

For the purpose of comparisons two sets of M field pressures has been used: a set with $M = N$ and a set with $M = 2N$. In the case of $M = N$, Gaussian elimination with partial pivoting is employed as linear solver and compared with the SVD solution using Tikhonov regularization. When $M = 2N$, least-squares with QR-Factorization is applied and similarly compared with the Tikhonov solution. The relative norm error is considered as indicated in [11]:

$$\text{error}(\%) = \frac{\|(\mathbf{p}_S, \mathbf{v}_S) - (\mathbf{p}_X, \mathbf{v}_X)\|}{\|(\mathbf{p}_S, \mathbf{v}_S)\|} \times 100 \tag{9}$$

where $\mathbf{p}_X$ and $\mathbf{v}_X$ are respectively the surface sound pressures and velocities estimated by the inverse process. $\|\cdot\|$ denotes the 2-norm. Figures 6 and 7 show the amplitudes and phase reconstructions as well as the computation times achieved by each solver. An example of the recovered impedances by least-squares at a test frequency of 210 Hz and $M = 2N$ is also shown in Figure 4, where the real and imaginary parts have been plotted element-wise for a better appreciation. Figure 5 shows in a similar way the estimated surface pressures and velocities of the same example.

As can be seen in Figure 5, a low percentage of error was obtained in the solutions given by the overdetermined least-square. The relative error of surface pressures remains under 1% in all the elements and in most of the surface velocities. From Figure 4, it can be seen that the recovered acoustic impedances are nearly the same as the actual values assigned manually. Nonetheless, we note from these results that even when low error levels in surface pressures and velocities where achieved, the reconstruction of impedances is more sensitive to errors since the impedance is given by the relationship of both the surface pressure and particle

Surface	**Material**	**Impedance** ($\times 10^6$ Rayls)	**Relative Impedance** (air: $Z_0 = 415$ Rayls)
floor	Wood	1.5	3,614
walls	Concrete	8	19,277
windows	Glass (8 mm)	13	31,325
door	Aluminum	17	40,964

Table 1: Assignment of acoustic impedance values for the simulations with the office room.

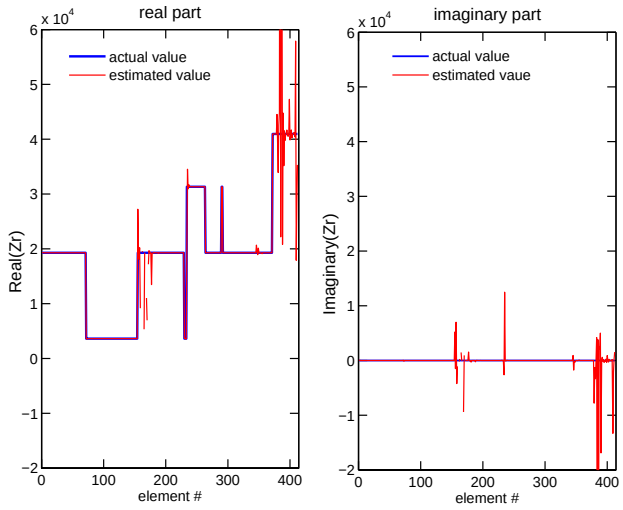

Figure 4: Relative impedances in the surfaces of the office room at 210 Hz.

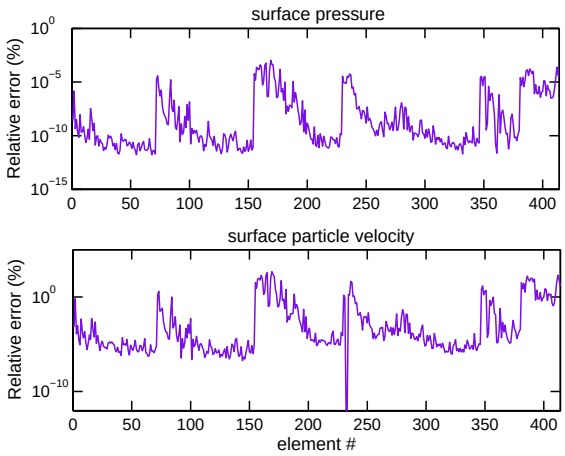

Figure 5: Reconstructed surface pressures and particle velocities of the office room at 210 Hz.

velocity. The elements where erroneous impedance was obtained can be observed easily by looking at the imaginary part of the estimated impedances of Figure 4 in which the original value is zero. Regarding this, it has been already mentioned in [8] and [16] that these errors are closely related to the complexity of the geometry. We will show that in addition the errors also vary according to the mesh quality.

With respect to the results in Figures 6 and 7, the following observations can be made:

- The error in reconstruction of velocity always keeps a higher level than that of the error of surface pressure. However, these levels of error tend to decrease as the analysis frequency increases. This tendency can be observed more evidently in the relative norm error of amplitude in Figure 6 with $M = N$. Previous work in the inverse radiation problem with NAH has also pointed out this effect and it was mentioned in [11] with studies on an interior problem.

- In the case when $M = N$ (i.e. number of field pressures p_f is equal the number of elements in the mesh), Tikhonov regularization shows lower error levels than Gaussian elminiation. However after about 110 Hz (i.e. $\lambda/d \approx 18$, with d =max. size of the elements), the performance of Gaussian elimination tends to get closer to the one of Tikhonov regularization, being the first in addition approximately 30 times faster than the second. Recall that Tikhonov method involves SVD analysis which in turn is expensive.

- When a number of field pressures bigger than the number of elements is considered (e.g. $M = 2N$), least-square approach (QR-factorization was used in the present work) gives similar performance to Tikhonov method and is approximately 7 times faster.

3.2 Basic geometry: unit cube

In this section we study two factors that affect the accuracy in the estimation of the acoustic impedance on the boundaries: the vibration mode and the mesh quality of the geometry. The effects of the complexity of the geometry over the reconstruction of boundary parameters for a radiation problem have been investigated in detail by Nelson and Yoon, [8], [9], and the influence of the resonance modes on the ill-condition of an interior problem was mentioned also by Kim and Ih, [11]. We adopted a basic geometry of an enclosed surface (a unit cube) in order to perform further studies and be able to appreciate the effects of the two mentioned factors over the accuracy.

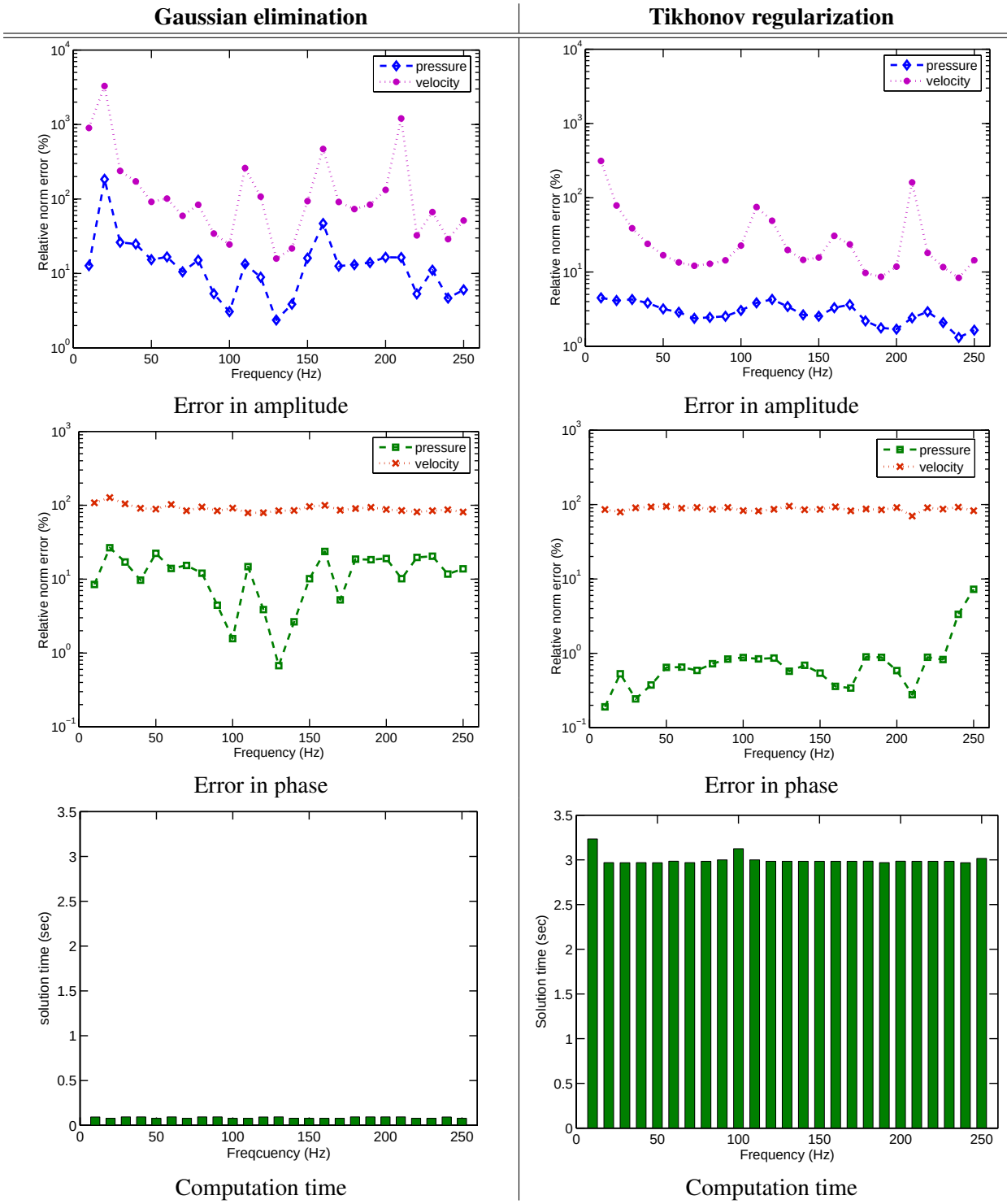

Figure 6: Recovered sound pressures and velocities with $M = N$ field samples in the office room simulations.

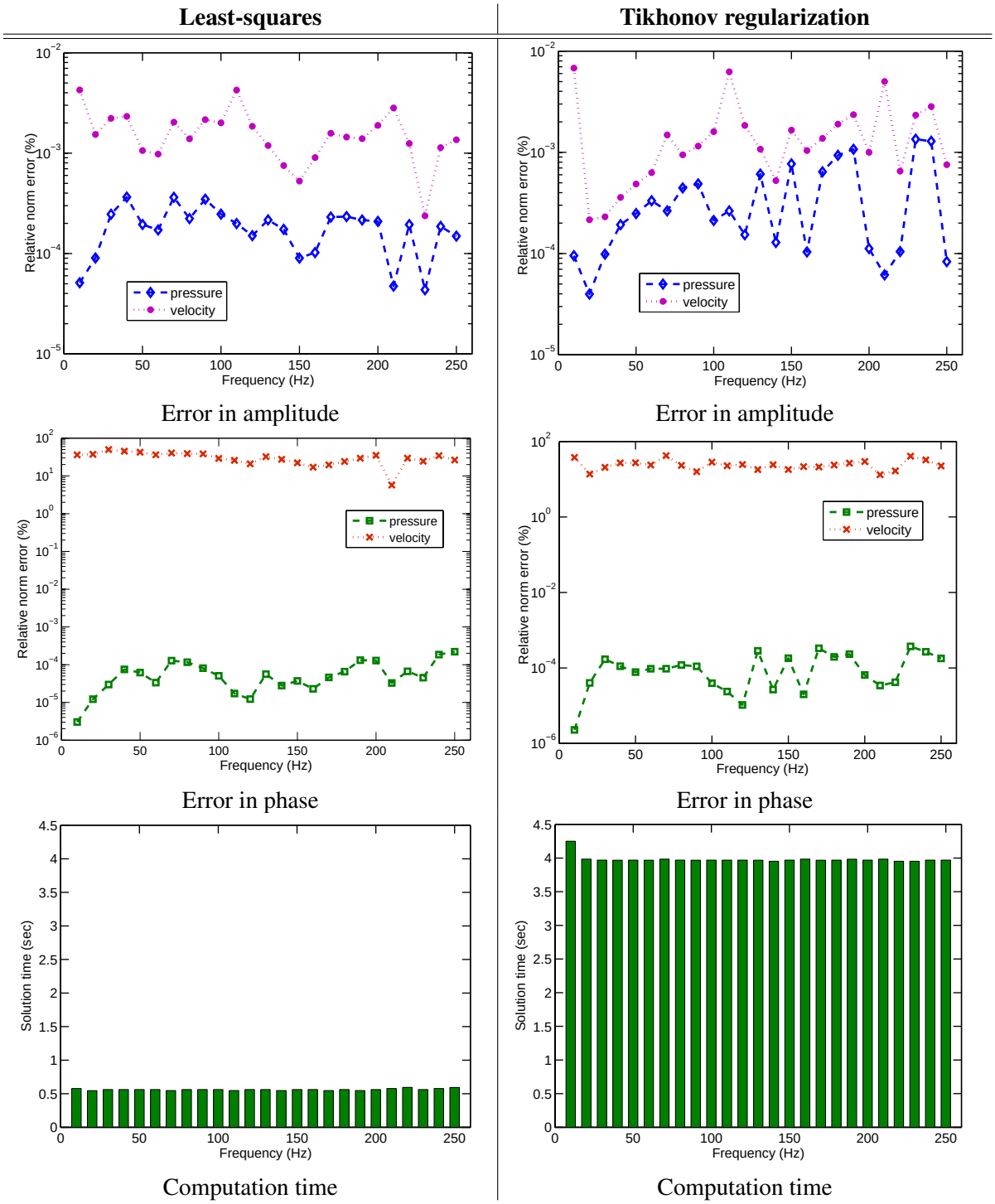

Figure 7: Recovered sound pressures and velocities with $M = 2N$ field samples in the office room simulations.

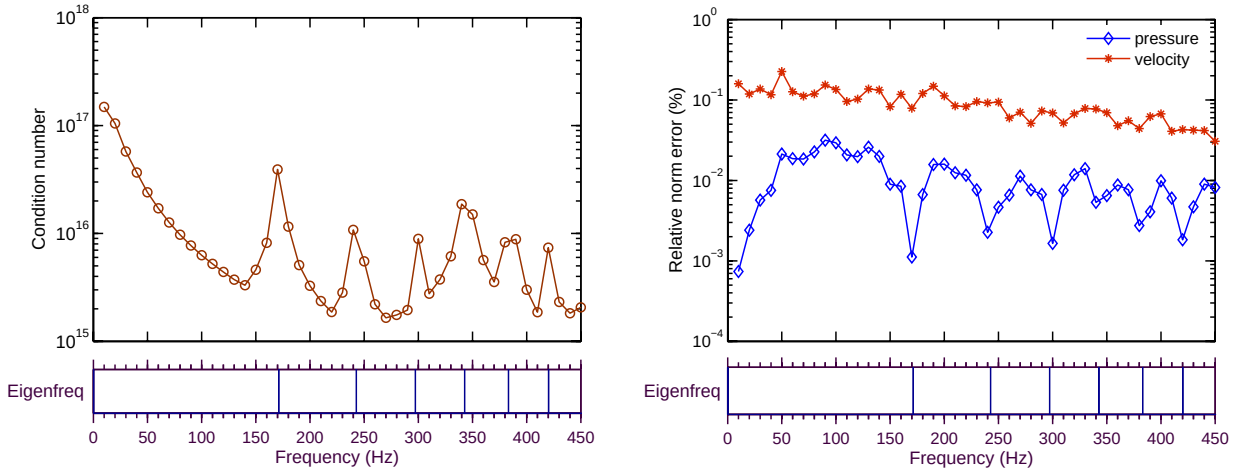

(a) (b)

Figure 8: Effects of the vibration modes over the inverse estimation accuracy. (a) Condition number vs. eigenfrequencies. (b) Relative norm error vs. eigenfrequencies.

3.2.1 Effects of the vibration modes

The unit cube is meshed into 432 triangular elements with almost uniform size, allowing a maximum analysis frequency of 282 Hz considering the $1/6$ wavelength criterion. The number of field pressures is fixed at $M = 2N$ and they are calculated at random points in the field using the BEM process by assigning concrete impedances (8×10^6 Rayls) to the boundaries, except one element of the mesh which is vibrating with an amplitude of 1 m^3/s to simulate the sound source. This procedure is repeated for a frequency range 10–450 Hz spaced by 10 Hz. The set of field pressures is used to solve the inverse process with least-squares and the surface pressures and velocities are estimated. Again, noiseless field pressures are taken since we wish to investigate the errors introduced by the system itself.

From the results of this test, we observe that the condition number of the linear system takes maximum values at the eigenfrequencies associated with the cube, as shown in Figure 8(a) where the eigenfrequencies have been aligned to the bottom of the graphs for a better comprehension. Although the condition number shows a decreasing tendency at high frequencies, the eigenfrequencies become denser at that range. Here, the condition number of the matrix **D** of equation (8) is calculated as in [8]:

$$k(D) = \|D\|\|D^{-1}\| \tag{10}$$

where $\|\cdot\|$ denotes the 2-norm. The norm error of the reconstruction seems not to be affected by the vibration modes of the geometry. Moreover, the error levels in surface pressure presented minima at the eigenfrequencies. This last effect has not been studied yet in this work but it will be a subject of investigation for the future. We observed that in the absence of noise the vibration modes mostly affect the way the errors are distributed in the geometry. Figure 9 shows an example of an error pattern produced by one of the resonance frequencies of the cube.

3.2.2 Effects of the mesh quality

Another effect that was observed during preliminary simulations is the tendency of the error to increase as the size of the mesh elements is less uniform. In order to investigate this effect, the unit cube is employed again and an analysis frequency that does not fall in any of the eigenfrequencies is chosen. The same boundary conditions used in the previous simulations with the cube are applied, but this time the area of a group of elements in the mesh is varied manually at each test, as illustrated in Figure 10. We define therefore the mesh

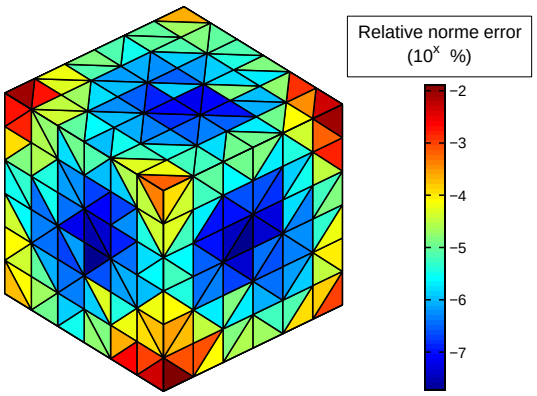

Figure 9: Example of an error pattern produced by a vibration mode at 243 Hz.

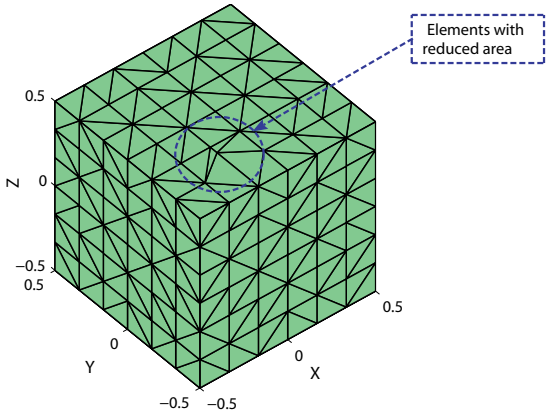

Figure 10: Mesh variations for the mesh quality test.

quality factor Q as follows:

$$Q = \frac{max(\text{element area})}{min(\text{element area})} \tag{11}$$

thus the behavior of the errors can be appreciated in terms of the mesh quality factor. Taking $M = N$ field pressures uniformly distributed inside the cube, we proceed to solve the inverse system with least-squares. The results of this tests are presented in Figures 11(a) and 11(b).

It became clear that the error in the inverse estimation of surface pressures and velocities is also affected by variations in the uniformity of the mesh elements, with a tendency to increase as one or more of the elements become considerably smaller with respect to the others. This variation can be explained in terms of the numerical computations of the integrals in the acoustic BEM. Recalling that the solution of the integral equations of the Kirchhoff-Helmholtz formulation by the BEM [16] involve the calculation of singular integrals of the forms:

$$\int_S f(\vec{r})\partial_n \left(\frac{e^{-jkr}}{4\pi r}\right) dS, \qquad \text{and} \qquad \int_S g(\vec{r}) \left(\frac{e^{-jkr}}{4\pi r}\right) dS$$

where the factors $1/r^2$ and $1/r$ represent the source of the singularity. In practice, these integrals are usually approximated with numerical techniques such as Gaussian quadrature with a transformation to polar coordinates. Therefore as the surface of the integrating element becomes infinitely small, the singularity of the integrand increases making the approximation of the integral inaccurate. This inaccuracy is propagated when performing the inverse process resulting in large errors in the reconstruction of p_S and v_S.

As the plots of Figures 11(a) and 11(b) suggest, there should be an optimum size of the elements that can produce the best reconstruction error in the sense of the least-squares. Hence, this optimum should be considered as well in the solution of the inverse estimation problem in order to improve the accuracy. However, this optimization process is out of the scope of the present work.

4 Future work

4.1 Improvements to the least-square solution

A priori knowledge of the distribution of the surfaces inside a given geometry (e.g. the surfaces in a room) may be exploited in order to incorporate extra information about the desired solution in the inverse esti-

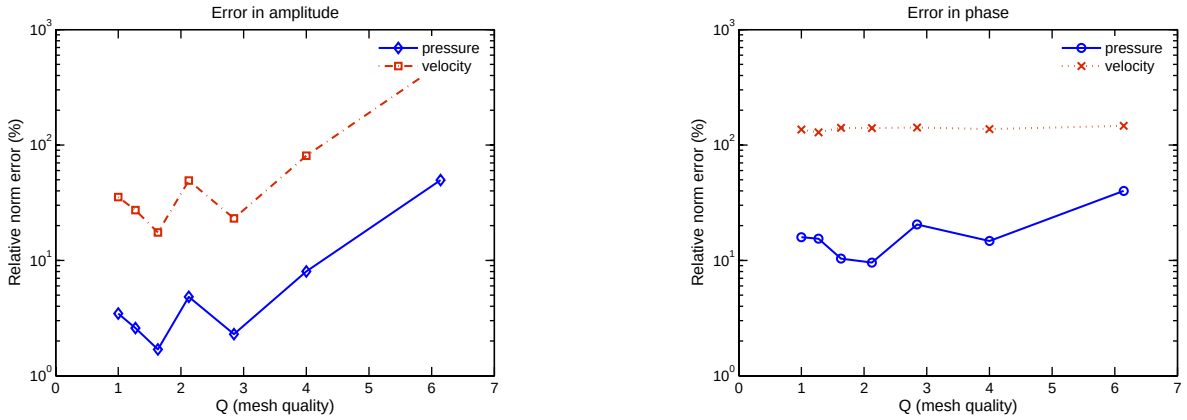

(a) (b)

Figure 11: Variation of the reconstruction error with the mesh quality. (a) Error in amplitude. (b) Error in phase.

mation. Thus, an additional constraint can be imposed on the least-square problem derived from equation (8).

Let k_i be the acoustic impedance uniformly distributed over each surface S_i, with $i = 1, 2, ..., n$, as illustrated in Figure 1. If we assume that the surfaces have homogeneous impedance value, the relation

$$z_{S_i,j} = \frac{p_{S_i,j}}{v_{S_i,j}} = \mathrm{k}_i \qquad\qquad j = 1, 2, ..., m \tag{12}$$

i.e. the impedance z of the j-th element of surface S_i, should satisfy

$$\frac{p_{S_i,1}}{v_{S_i,1}} = \frac{p_{S_i,2}}{v_{S_i,2}} = ... = \frac{p_{S_i,m}}{v_{S_i,m}} = \mathrm{k}_i \tag{13}$$

Since k_i is constant and uniform on S_i, taking the differential of the impedance with respect to the surface yields

$$\frac{d[z_i]}{dS_i} = \frac{d}{dS_i}\left[\frac{p_{S_i}}{v_{S_i}}\right] = \frac{d[\mathrm{k}_i]}{dS_i} = 0 \tag{14}$$

In the actual meshed model the surfaces S_i are discretized into m elements, so we can state an equivalent condition to expression (14) as follows:

$$f_{S_i}(z) = \sum_{j=1}^{m_i-1} (z_{S_i,j+1} - z_{S_i,j}) = 0 \tag{15}$$

There are n different surfaces in the model, thus we have n equations in the form:

$$f_{S_1}(z) = \sum_{j=1}^{m_1-1} (z_{S_1,j+1} - z_{S_1,j}) = 0$$

$$f_{S_2}(z) = \sum_{j=1}^{m_2-1} (z_{S_2,j+1} - z_{S_2,j}) = 0$$

$$\vdots$$

$$f_{S_n}(z) = \sum_{j=1}^{m_n-1} (z_{S_n,j+1} - z_{S_n,j}) = 0$$

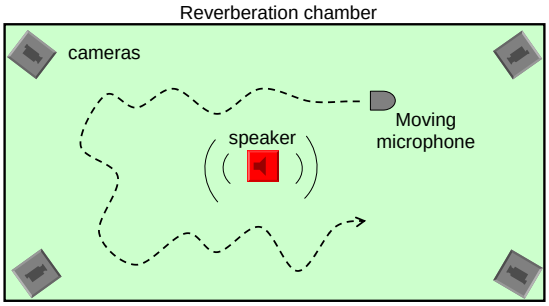

Figure 12: Preliminary setup for validation experiments.

Or expressed in the matrix form

$$\mathbf{f}(\mathbf{z}) = \mathbf{G}\mathbf{z} = \mathbf{0} \tag{16}$$

where

$$\mathbf{G} = \begin{pmatrix} \mathbf{H}_{S_1} & \mathbf{0} & \cdots & \cdots & \mathbf{0} \\ \mathbf{0} & \mathbf{H}_{S_2} & \mathbf{0} & & \vdots \\ \vdots & & \ddots & & \vdots \\ \vdots & & & \ddots & \mathbf{0} \\ \mathbf{0} & \cdots & \cdots & \mathbf{0} & \mathbf{H}_{S_n} \end{pmatrix} \quad , \quad \mathbf{H}_{S_i} = \begin{pmatrix} -1 & 1 & 0 & \cdots & \cdots & 0 \\ 0 & -1 & 1 & 0 & \cdots & 0 \\ \vdots & & \ddots & \ddots & & \vdots \\ \vdots & & & \ddots & \ddots & \vdots \\ 0 & \cdots & \cdots & 0 & -1 & 1 \end{pmatrix}$$

$$\mathbf{z} = [z_{S_1,1} \cdots z_{S_1,m_1} \;\; , \;\; z_{S_2,1} \cdots z_{S_2,m_2} \;\; , \;\; \cdots \;\; , \;\; z_{S_n,1} \cdots z_{S_n,m_n}]^T$$

The dimension of the matrices $\mathbf{H}_{S_i}$ is $(m_i - 1) \times m_i$. We can now use equation (8) and the condition (16) to solve a weighted least-square problem. Moreover, extra assumptions about the impedance of the surfaces in relation to the impedance of the acoustic field can allow us to impose boundaries to the solution sought. The optimization problem is then given by:

$$\min_{\mathbf{x}_S} \quad g(\mathbf{x}_S) = \|\mathbf{D}\,\mathbf{x}_S - \mathbf{d}\|^2 + \lambda \|\mathbf{G}\,\mathbf{z}(\mathbf{x}_S)\|^2 \tag{17}$$

$$\text{with} \qquad Z_0 < \mathbf{z}(\mathbf{x}_S) < Z_{max}$$

In the future studies, simulations using the derived weighted-least-squares will be performed to compare results with those already obtained here.

4.2 Experimental validation

We will attempt to estimate the acoustic impedance on the surfaces of a real model by taking sound pressure samples in the interior of a reverberation chamber. In order to perform the inverse estimation using the method presented in this work, it is necessary to take at least as many samples as the number of elements in the mesh of the model. To overcome this problem and be able to take samples at random locations, we will introduce the use of stereo vision with cameras to track in real-time the 3D position of the measuring microphone which will be freely moving in the interior space. Thus we can continuously take samples of sound as the microphone moves. Figure 12 shows the preliminary setup for the experimentation stage. Care should be taken since the speed at which the microphone will move is restricted by the wavelength of the analysis frequency. Details on the implementation of the measurement system will be given in a future report. By that time, the effects of noise in the field pressures and deviations in the 3D position of the measurement points will be considered in order to investigate their influence over the accuracy.

5 Conclusions

The inverse boundary element method (IBEM) applied to in-situ estimation of acoustic impedance of the surfaces in interior spaces has been studied. The scaled model of an office room was used for numerical simulations as a realistic example of the applicability of our method to complex geometries . A simpler geometry (unit cube) was also employed in order to investigate the influence of the eigenfrequencies and the mesh quality over the accuracy of the estimation.

Results obtained using the inverse formulation derived here show that when the number of field pressures equals the number of elements, Tikhonov regularization mantains better levels of error than Gaussian elimination with the cost of expensive computational effort. However, at the range of higher frequencies (e.g. $\lambda/d \leq 18$ for the unit cube) and when the noise level is almost null, Gaussian elimination can represent a satisfactory solution in terms of computational efficiency. For the case of an overdetermined system (e.g. $M \geq 2N$), least-squares performs nearly similar to Tokhonov regularization with less computation time. In principle when dealing with certain levels of noise in the data, least-squares would give a reasonable solution if the system is sufficiently overdetermined.

Considering the results reported in previous work and those shown here we can infer that the vibration modes associated with the geometry affect the error levels of reconstruction if there is noise in the data, and those errors are transmitted via the singular values of the linear system. The quality of the mesh is another factor that influence the estimation accuracy. The balance between the sizes of the elements represents an optimization problem to be considered in order to achieve improvements on the inverse estimation. This may be a difficult point to satisfy since until now there are no available systems that provide full control over the mesh generation process.

In-situ measurement of acoustic properties of materials remains as an active subject of research. A system that allow us to estimate the acoustic impedance of the surfaces of an entire space by taking samples of sound at random places in the field will greatly help in several fields of acoustic design. Although the method proposed here can be used in different acoustic areas, the current target application is sound rendering of virtual reality environments for the production of realistic sound fields.

References

[1] C. Noke, V. Mellert, *Breif review on in situ measurement techniques of impedance or absorption*, Forum Acusticum, Sevilla (2002).

[2] J.D. Maynard, E.G. Williams, Y. Lee, *Nearfield acoustic holography: I. Theory of generalized holography and the developement of NAH*, Journal of the Acoust. Soc. Amer., Vol. 78, No.4, (1985), pp. 1395-1413.

[3] W.A. Veronesi, J.D. Maynard, *Nearfield acoustic holography: II. Holopraphic reconstruction algorithms and computer implementation*, Journal of the Acoust. Soc. Amer., Vol. 81, No.5, (1987), pp. 1307-1322.

[4] W.A. Veronesi, J.D. Maynard, *Digital holographic reconstruction of sources with arbitrarily shaped surfaces*, Journal of the Acoust. Soc. Amer., Vol. 85, No.5, (1989), pp. 588-598.

[5] G.V. Borgiotti, E. M. Rosen, *The determination of the far field of an acoustic radiator from sparse measurement samples in the near field*, Journal of the Acoust. Soc. Amer., No.92, (1992), pp. 807-818.

[6] J.Hald, *STSF - a unique technique for scan-based near-field acoustic holography without restrictions of coherence*, *Brel and Kjr Technical Review*, No.1, (1989), pp. 1-49.

[7] M.R. Bai, *Application of BEM (boundary element mehtod)- based acoustic holography to radiation analysis of sound sources with arbitrarily shaped geometries*, Journal Acoust. Soc. Amer., No.92, (1992), pp. 533-548.

[8] P.A. Nelson, S.H. Yoo, *Estimation of acoustic source strength by inverse methods: Part I, conditioning of the inverse problem*, Journal of Sound and Vibration, No.233, (2000), pp. 643-668.

[9] S.H. Yoo, P.A. Nelson, *Estimation of acoustic source strength by inverse methods: Part II, experimental investigation of methods for choosing regularization parameters*, Journal of Sound and Vibration, No.233, (2000), pp. 669-705.

[10] B.-K. Kim, J.-G. Ih, *Reconstruction of vibro-acoustic field of car panels using acoustic BEM*, Proc. Inter-Noise 95, (1995), pp. 1341-1344.

[11] B.-K. Kim, J.-G. Ih, *On the reconstruction of the vibro-acoustic field over the surface enclosing and interior space using the boundary element method*, Journal Acoust. Soc. Amer., Vol.100, No.5, (1996), pp. 3003-3016.

[12] P.J.T. Fillipi, D. Habault, J. Piraux, *Noise source modeling and identification procedure*, Journal of Sound and Vibration, No.124, (1988), pp. 285-296.

[13] D.M.Photiadis, *The relationship of singular value decomposition to wave-vector filtering in sound radiation problems*, Journal Acoust. Soc. Amer., Vol.88, No.2, (1990), pp. 1152-1159.

[14] G.T. Kim, B.H Lee, *3D sound reconstruction and field projection using the Helmholtz integral equation*, Journal of Sound and Vibration, No.136, (1990), pp. 245-261.

[15] A.N.Tikhonov, *Solution of incorrectly formulated problems and the regularization method*, Soviet Math. Dokl., No.4, (1963), pp. 1035-1038.

[16] O. von Estorff, *Boundary elements in acoustics - Advances and applications*, WIT Press, (2000).

[17] *Signal Processing SA*, http://www.signal-processing.com/tech/us_data_frame.htm

[18] G. Patow, *A survey of inverse rendering problems*, Computer Graphics Forum, Vol. 22, No.4, (2003), pp. 663-667.